nature portfolio

https://doi.org/10.1038/s41567-022-01514-1

Supplementary information

Fermi surface transformation at the pseudogap critical point of a cuprate superconductor

In the format provided by the authors and unedited

Supplementary Information: Fermi surface transformation at the pseudogap critical point of a cuprate superconductor

Yawen Fang,[1,*] Gaël Grissonnanche,[1,2,3,*] Anaëlle Legros,[3,4] Simon Verret,[3] Francis Laliberté,[3] Clément Collignon,[3] Amirreza Ataei,[3] Maxime Dion,[3] Jianshi Zhou,[5] David Graf,[6] M. J. Lawler,[7,1] Paul A. Goddard,[8] Louis Taillefer,[3,9] and B. J. Ramshaw[1,9,†]

[1]*Laboratory of Atomic and Solid State Physics, Cornell University, Ithaca, NY, USA*

[2]*Kavli Institute at Cornell for Nanoscale Science, Ithaca, NY, USA*

[3]*Département de physique, Institut quantique, and RQMP, Université de Sherbrooke, Sherbrooke, Québec, Canada*

[4]*SPEC, CEA, CNRS-UMR 3680, Université Paris-Saclay, Gif sur Yvette Cedex, France*

[5]*Materials Science and Engineering Program, Department of Mechanical Engineering, University of Texas at Austin, Austin, TX, USA*

[6]*National High Magnetic Field Laboratory, FL, USA*

[7]*Department of Physics, Applied Physics and Astronomy, Binghamton University, Binghamton, New York, USA*

[8]*Department of Physics, University of Warwick, Coventry, UK*

[9]*Canadian Institute for Advanced Research, Toronto, Ontario, Canada*

Crystal structure of Nd-LSCO at $p = 0.21$ and $p = 0.24$

Recent dilatometry measurements have been performed on samples cut from the same larger samples as the ones we have measured here (see Extended Data Figure 7 in Grissonnanche *et al.* [1]). These measurements show that both the $p = 0.21$ and $p = 0.24$ samples transition from the low-temperature-orthorhombic (LTO) to the low-temperature-tetragonal (LTT) phase at $T_{\rm LTT} = 75$ K ($p = 0.21$) and $T_{\rm LTT} = 50$ K ($p = 0.24$) [2]. This means that our three samples of Nd-LSCO ($p = 0.20, 0.21$, and 0.24) have the same structure (LTT) at the temperature of our experiment ($T = 25$ K). This fact has recently been confirmed by detailed X-ray and neutron measurements [3].

Nd-LSCO $p = 0.24$: Yamaji angle analogy

An intuitive picture for interpreting the structure of ADMR is that minima in the conductivity (maxima in the resistivity) occur at angles where a component of the Fermi velocity averages toward zero for most of the cyclotron orbits. In a quasi-2D material with a simple sinusoidal dispersion along the k_z direction and $\omega_c\tau \gg 1$, the ADMR has peaks at θ values corresponding to zeros of $J_0(ck_F \tan\theta)$, where $J_0(x)$ is the 0^{th} order Bessel function of the first kind, c is the interlayer lattice constant, and k_F is the average Fermi wavevector [4]. These special angles are referred to as Yamaji angles—at these angles all Fermi surface cross-sectional areas are equal and the c-axis Fermi velocity (v_z) averages to zero for all cyclotron orbits [5].

For Nd-LSCO at $p = 0.24$, the Fermi surface along the k_z direction is more complicated than a simple sinusoidal warping and the material is also far from the $\omega_c\tau \gg 1$ limit. Similar intuition to the simple Yamaji angle scenario, however, still holds at low θ. While there are no longer angles where v_z averages to precisely to zero for all cyclotron orbits there are still angles where the orbital average of v_z is minimal. At these same angles where the orbitally-averaged v_z is minimal the cyclotron orbits all have similar areas. This means that the rate of change of area as one moves along k_z is a minimum at certain angles, and these angles correspond to maxima in the resistivity.

As shown in Figure S1, the variation in the cyclotron orbit area drops to a minimum at around 32° for $\phi = 0°$. This is near the angle where we find a peak in the ADMR for $p = 0.24$, indicating that this angle is indeed one where v_z is averaged close to zero most effectively. In addition, as ϕ is rotated toward 45°, the minimum in rate of change of the area moves to lower θ, tracking the behaviour of the peak in the ADMR (the lifetime τ has been increased for the calculated ADMR in Figure S1c to highlight the peak.) Thus, while the interlayer warping of Nd-LSCO is not a simple sinusoid, and $\omega_c\tau \ll 1$, the Yamaji-angle picture still provides the correct intuition for interpreting the ADMR.

Nd-LSCO $p = 0.21$: YRZ Fermi surface reconstruction

There are alternative routes to producing nodal hole pockets similar to what is produced by a ($\boldsymbol{\pi}$,$\boldsymbol{\pi}$) reconstruction. One example is the Yang, Rice, and Zhang (YRZ) ansatz [6],

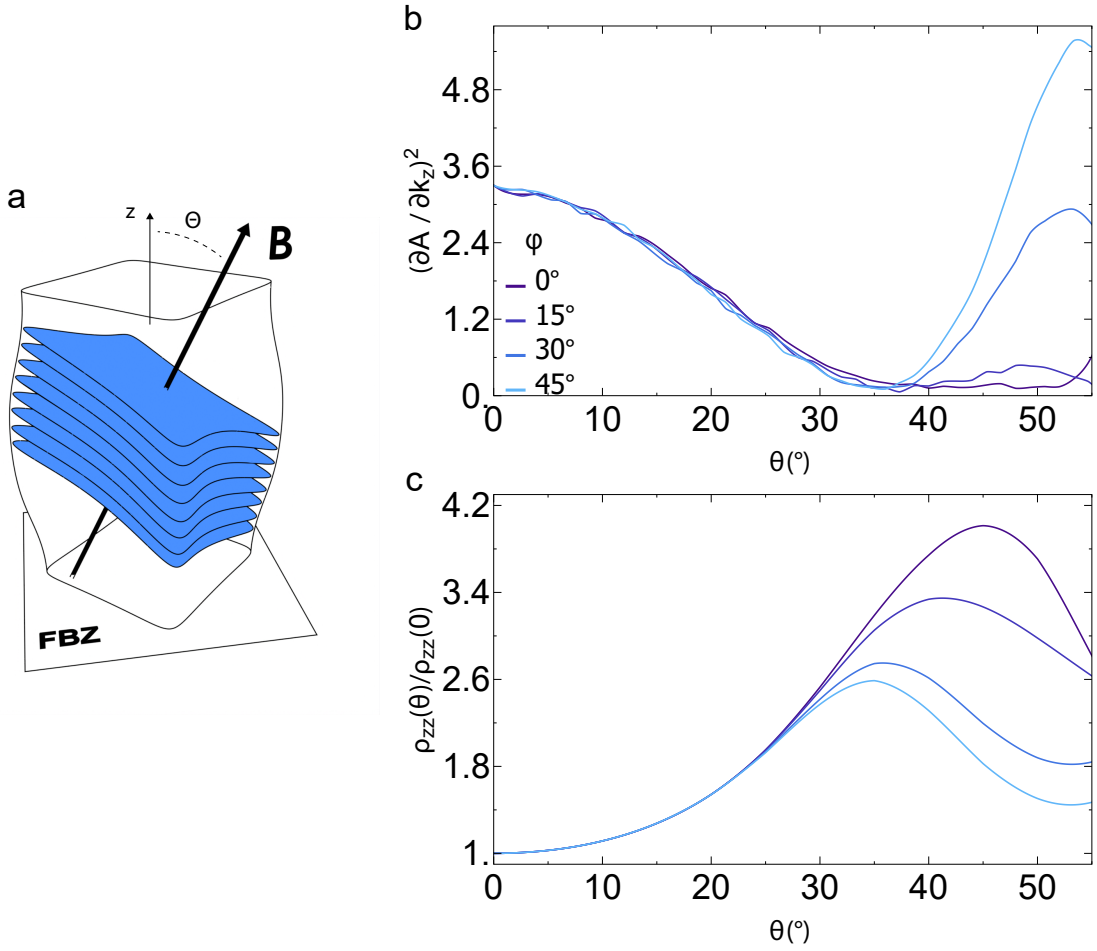

FIG. S1. **Cross-sectional area of the cyclotron orbits as a function of angle.** (**a**) The Fermi surface of Nd-LSCO $p = 0.24$ in the first Brillouin zone. The black arrow represents the direction of the magnetic field $\boldsymbol{B}$. Each blue surface represent the area enclosed by a cyclotron orbit for this particular direction of $\boldsymbol{B}$ (here just a few orbits are shown as examples). (**b**) The square of the rate-of-change of Fermi surface area as a function of k_z: when this quantity is zero it means that all orbits have the same area. (**c**) ADMR calculated for the FS shown in (a) with $\omega_c\tau$ chosen to be long enough to emphasize the peaks in the resistivity where there are minima in panel (b).

which has been shown to reproduce the decrease in the Hall coefficient below $p^\star$ [7].

The tight binding model for the YRZ ansatz is

$$\epsilon_{\mathrm{YRZ}}(k_x,k_y,k_z) = \frac{1}{2}\left(\xi_k+\xi_k^0\right) - \sqrt{\left(\frac{\xi_k+\xi_k^0}{2}\right)+E_g^2(k_x,k_y,k_z)} \\ - 2t_z\cos\left(\frac{k_z c}{2}\right)\cos\left(\frac{k_x a}{2}\right)\cos\left(\frac{k_y a}{2}\right)\left[\cos(k_x a)-\cos(k_y a)\right]^2, \tag{1}$$

where ξ_k, ξ_k^0, and E_g are given by

$$\xi_k = -2t\left[\cos(k_x a)+\cos(k_y a)\right] - 4t'\cos(k_x a)\cos(k_y a) \\ - 4t''\left[\cos(2k_x a)+\cos(2k_y a)\right] - \mu \tag{2}$$

$$\xi_k^0 = -2t\left[\cos(2k_x a)+\cos(2k_y a)\right] \tag{3}$$

$$E_g = \Delta/2\left[\cos(2k_x a)-\cos(2k_y a)\right]. \tag{4}$$

As was the case with the ($\boldsymbol{\pi}$,$\boldsymbol{\pi}$) reconstruction, we select only the nodal hole pockets because of their consistency with the measured Hall effect, and introduce the interlayer coupling after in-plane reconstruction. The resulting nodal hole pockets are shown in Figure S2a, and the best fit is shown in Figure S2c. The best fit parameters are an isotropic scattering rate of $1/\tau = 26$ ps^{-1}, $\mu = -0.492t$, $t_z = 0.278t$, and $\Delta = 0.013t$, with the rest of the tight binding parameters taken from Extended Data Table 1.

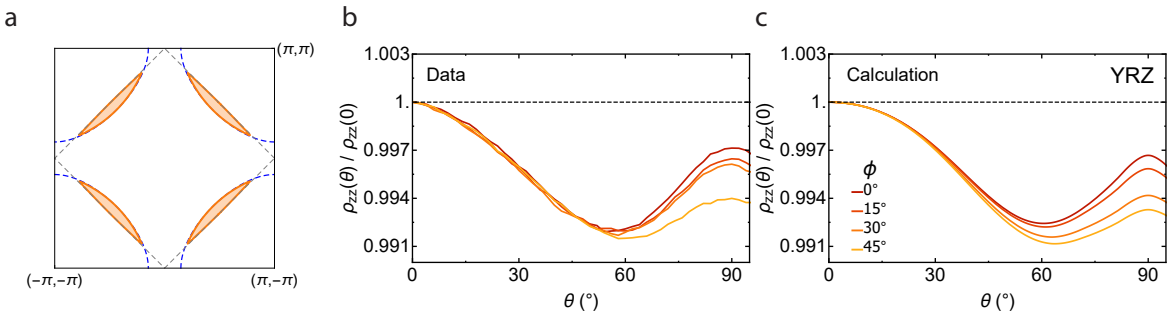

FIG. S2. **Fermi surface reconstruction by the YRZ ansatz.** (**a**) The nodal hole pockets produced by the YRZ reconstruction. (**b**) The ADMR data for $p = 0.21$, reproduced from Figure 1c in the main text. (**c**) Best-fit of the ADMR using the YRZ model and a constant scattering rate.

Nd-LSCO $p = 0.20$: ADMR data

We performed ADMR measurements on Nd-LSCO at $p = 0.20$ ($< p^*$), as shown in Figure S3. Due to time constraints on the 45 Tesla hybrid at the National Magnet Lab in Tallahassee, data at this doping were only taken for two different ϕ values. The data are similar to Nd-LSCO $p = 0.21$, but with a less pronounced anisotropy in ϕ around $\theta = 90°$.

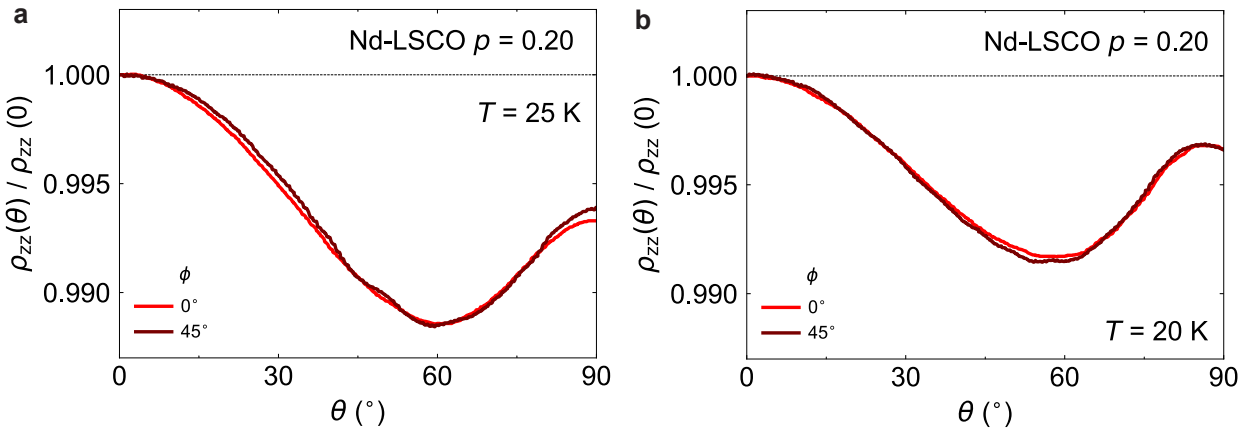

FIG. S3. **ADMR data of Nd-LSCO $p = 0.20$.** ADMR data at $B = 45$ T as a function of θ, for $\phi = 0°$ and 45°. (**a**) $T = 25$ K; (**b**) $T = 20$ K.

---

* These authors contributed equally to this work

† To whom correspondence should be addressed, bradramshaw@cornell.edu

[1] G. Grissonnanche, S. Thériault, A. Gourgout, M.-E. Boulanger, E. Lefrançois, A. Ataei, F. Laliberté, M. Dion, J.-S. Zhou, S. Pyon, T. Takayama, H. Takagi, N. Doiron-Leyraud, and L. Taillefer, Chiral phonons in the pseudogap phase of cuprates, Nature Physics **16**, 1108 (2020).

[2] G. Grissonnanche, A. Legros, S. Badoux, E. Lefrançois, V. Zatko, M. Lizaire, F. Laliberté, A. Gourgout, J.-S. Zhou, S. Pyon, *et al.*, Giant thermal hall conductivity in the pseudogap phase of cuprate superconductors, Nature **571**, 376 (2019).

[3] M. Dragomir, Q. Ma, J. P. Clancy, A. Ataei, P. A. Dube, S. Sharma, A. Huq, H. A. Dabkowska, L. Taillefer, and B. D. Gaulin, Materials preparation, single crystal growth, and the phase diagram of the cuprate high temperature superconductor $La_{1.6-x}Nd_{0.4}Sr_xCuO_4$ (2020).

[4] K. Yamaji, On the angle dependence of the magnetoresistance in quasi-two-dimensional organic superconductors, Journal of the Physical Society of Japan **58**, 1520 (1989).

[5] C. Bergemann, S. Julian, A. Mackenzie, S. NishiZaki, and Y. Maeno, Detailed topography of the fermi surface of Sr_2RuO_4, Physical review letters **84**, 2662 (2000).

[6] T. M. Rice, K.-Y. Yang, and F.-C. Zhang, A phenomenological theory of the anomalous pseudogap phase in underdoped cuprates, Reports on Progress in Physics **75**, 016502 (2011).

[7] J. Storey, Hall effect and fermi surface reconstruction via electron pockets in the high-T_c cuprates, EPL (Europhysics Letters) **113**, 27003 (2016).